Energy & Environmental Science

ROYAL SOCIETY OF CHEMISTRY

PAPER

View Article Online
View Journal

Cite this: DOI: 10.1039/d3ee01156a

Self-powered recycling of spent lithium iron phosphate batteries *via* triboelectric nanogenerator†

Baofeng Zhang,[ab] Lixia He,[ab] Jing Wang,[ab] Yuebo Liu,[ad] Xu Xue,[e] Shengnan He,[e] Chuguo Zhang,[ab] Zhihao Zhao,[ab] Linglin Zhou,[ab] Jie Wang *[abd] and Zhong Lin Wang [acf]

Received 12th April 2023,
Accepted 21st July 2023

DOI: 10.1039/d3ee01156a

rsc.li/ees

The recycling of lithium iron phosphate batteries (LFPs), which represent more than 32% of the worldwide lithium-ion battery (LIB) market share, has raised attention owing to the valuable element resources and environmental concerns. However, state-of-the-art recycling technologies, which are typically based on electrochemical or chemical leaching methods, have critical issues such as tedious procedures, enormous chemical/electricity consumption and secondary pollution. Here, we report an innovative self-powered system composed of an electrochemical LIB recycling reactor and a triboelectric nanogenerator (TENG) for recycling spent LFP. In the electrochemical LIB recycling reactor, the Cl^-/ClO^- pair generated electrochemically in NaCl solution is adopted as the redox mediator to break down LFP into $FePO_4$ and Li^+ *via* the redox targeting reaction without extra chemicals. Additionally, a TENG that utilizes discarded components from LIBs including casings, aluminum-plastic films and current collectors is designed to drastically minimize secondary pollutants. Furthermore, the TENG harvests wind energy, delivering an output of 0.21 W for powering the electrochemical recycling system and charging batteries. Therefore, the proposed system for recycling spent LFP exhibits high purity (Li_2CO_3, 99.70% and $FePO_4$, 99.75%), self-powered features, simplified treatment procedure and a high profit, which can promote the sustainability of LIB technologies.

Broader context

The electrification of transportation, represented by electric vehicles, is an effective route for alleviating greenhouse gas emissions, mitigating atmospheric pollution and decarbonizing the energy system. Lithium-ion batteries (LIBs) with high energy density and power density strongly affect the driving performance of vehicles. Among the commercialized LIBs, lithium iron phosphate (LFP) batteries have attracted attention due to their structural stability, long service life, *etc.*, which in turn has led to an increased number of spent LIBs. Currently, there are three mainstream processes, pyrometallurgy, hydrometallurgy, and direct regeneration, for recycling spent LFP batteries. However, the direct regeneration process can hardly repair the broken structure, the pyrometallurgical process is hindered by its energy consumption, metal loss and hazardous gaseous emissions, and the hydrometallurgical process consumes large amounts of acid/alkali chemicals with complicated procedures. Here, we report a self-powered system for recycling spent LFP batteries, in which Cl^-/ClO^- is adopted to break down LFP into $FePO_4$ and Li^+ without extra chemical inputs, while discarded components from LIBs are further utilized to fabricate a TENG to minimize secondary pollutants. Furthermore, the TENG harvests wind energy to power the electrochemical recycling reactor. Therefore, the proposed system acquires high purity, self-powered features, a simplified procedure and high profit, which can promote the sustainability of LIB technologies.

[a] *Beijing Institute of Nanoenergy and Nanosystems, Chinese Academy of Sciences, Beijing 100083, P. R. China. E-mail: wangjie@binn.cas.cn*
[b] *College of Nanoscience and Technology, University of Chinese Academy of Sciences, Beijing 100049, P. R. China*
[c] *Georgia Institute of Technology, Atlanta, GA 30332, USA*
[d] *Center on Nanoenergy Research, School of Physical Science and Technology, Guangxi University, Nanning, 530004, P. R. China*
[e] *Institute of Science and Technology for New Energy, Xi'an Technological University, Xi'an 710021, China*
[f] *Yonsei Frontier Lab, Yonsei University, Seoul 03722, Republic of Korea*
† Electronic supplementary information (ESI) available. See DOI: https://doi.org/10.1039/d3ee01156a

Introduction

Actuated by the motivation toward the decarbonization of transportation, the electric vehicle (EV) stock has exploded from 17 thousand units in 2010 to 16.2 million units in 2021, according to the statistical data released by the International Energy Agency (IEA). Lithium ion batteries (LIBs), which have the advantages of high capacity and power density, are considered to be a key component that determines the driving

performance of overall vehicle.[1–4] Among the commercialized LIBs, lithium iron phosphate ($LiFePO_4$, LFP) batteries are widely used and represent more than 32% of the overall LIB market share owing to their superior safety, earth-abundant iron sources, and relatively low production costs. Although LFP is regarded as an ecofriendly material, its improper disposal will create serious environmental crises. Additionally, spent batteries represent a valuable resource, because the concentration of the critical elements, especially lithium, contained in spent LFP batteries exceeds that in minerals. For instance, producing one ton of lithium requires only ~23 tons of spent LFP batteries compared with 750 tons or 250 tons of the corresponding brine or ore.[5,6]

Typically, pyrometallurgy, hydrometallurgy, and the direct recycling process are commonly used for recycling LFP LIBs. Although the pyrometallurgical method has been commercialized to recycle spent ternary LIBs, it is not preferable for recycling LFP due to the stable structure of LFP at high temperature, the high energy consumption of the method, and low lithium recovery efficiency.[7] The hydrometallurgical method, in which the crystal structures of the LFP are decomposed to the element level, is widely used in light of its high recovery efficiency and high purity. Although many inorganic acids (such as sulfuric acid, phosphoric acid and hydrochloric acid) or organic acids (such as citric acid, oxalic acid, acetic acid, *etc.*) have been used to recycle spent LFP, complicated follow-up processing, such as neutralization of the acidic water with alkali, ball-milling processes to increase leaching efficiency, *etc.*, are required, which further increase the financial burden, energy consumption and the risk of secondary pollution.[8] Direct recycling is being studied to renovate LFP cathode materials without breaking down the crystal structure.[9] With the aim of solving the two main factors that lead to the degradation of LFP, lithium vacancy defects and Fe–Li anti-site defect, targeted healing methods,[10] molten salt processes,[11] pyrolysis of multifunctional organic lithium salts,[12] usage of a prelithiated separator,[13] and hydrothermal methods[14] have been adopted and found to partly revitalize the structure, composition, and electrochemical performance of the spent LFP cathode material. However, beyond the challenge of repairing the crystal structure of electroactive materials, the sluggish charge transport is also an inherent disadvantage due to the destruction of the conductive coating during the regeneration process.[12] Thus, the development of a simplified recycling strategy that provides chemical/energy savings while renewing the high electrochemical performance of recycled LFP is desired. Recently, a direct oxidation strategy that extracts the lithium in the solutions, resulting in $FePO_4$ (FP) precipitate, has been proposed to recover LFP batteries. Its simplified recycling procedure is similar to the charging of LFP batteries, greatly reducing the chemical consumption. Therefore, sodium persulfate ($Na_2S_2O_8$),[8] ammonium persulfate ($(NH_4)_2S_2O_8$),[15] potassium ferrocyanide ($K_3[Fe(CN)_6]$),[16] hydrogen peroxide (H_2O_2),[17] and sodium hypochlorite (NaClO),[18] among others, have been reported as mediator oxidants to selectively break down the material in high purity in the absence of acid. However, the consumption of these chemicals used is relatively high. Although the oxidants can be instantaneously regenerated using an electrochemical reaction to maintain the recycling process, a large amount of electricity is consumed. Furthermore, in the conventional recycling of LFP batteries, the casings, aluminum-plastic film, separators and even the anode are discarded as waste after dismantling, and thus the full recovery of LIBs cannot be acheived.[19,20] This may also lead to secondary pollution. Thus, it is urgent to find a way to achieve the full utilization of all abandoned parts and develop an energy harvester that can offer power supply in a sustainable, clean and self-powered manner.

Recently, triboelectric nanogenerators (TENGs) have attracted the attention of researchers as a cutting-edge technology, as they can harvest distributed mechanical energy into electricity by coupling the effects of electrification and electrostatic induction.[21] Based on TENGs, electrochemical hydrogen peroxide production systems,[22] corrosion prevention of metal in a marine environment,[23,24] seawater splitting to produce high-purity hydrogen,[25,26] organic contaminant degradation systems,[27,28] and biomedical applications[29] have been explored in self-powered mode. However, the innovative recycling of spent LIBs by forming a self-powered electrochemical system is still questionable. Additionally, utilizing the characteristics of wide material and structure selection, TENGs can fully utilize waste materials, like waste milk cartons,[30] discarded cigarette filters,[31] waste polymers,[32] recycled coffee waste,[33] and even waste tea leaves and packaging bags,[34] to harvest mechanical energy. Nevertheless, TENGs made from waste components from spent LIBs are seldom reported.

Here, a self-powered system composed of the electrochemical LIB recycling reactor and a TENG is proposed for recycling spent LFP with high purity, a simplified procedure and high profitability. In the electrochemical LIB recycling reactor, a Cl^-/ClO^- pair that is electrochemically generated in NaCl solution is adopted as the redox mediator to break down LFP into $FePO_4$ (FP) and Li^+ *via* the redox targeting reaction without extra chemicals. The TENG, benefiting from the wide selection of materials, utilizes discarded components including casings, aluminum-plastic films (APF) and current collectors from LIBs to drastically minimize secondary pollutants. Additionally, the fabricated TENG delivers an average output of 0.21 W by harvesting the wind energy for powering the electrochemical recycling system to realize self-powering ability. More importantly, based on a systematic investigation of the output performance of TENG to reveal the mechanism of the electrochemical recycling of LFP and the regeneration of LFP, and on an economic evaluation, the proposed self-powered recycling system for spent lithium-ion batteries exhibits ecological and economic advantages.

Results and discussion

Working mechanism of self-powered system for recycling spent LFP batteries

The self-powered system for recycling spent LFP batteries mainly consists of three parts (Fig. 1a): the recycling system for LFP batteries, the fabrication of a TENG and the self-powering of the recycling system. (1) Spent batteries from laptops, EVs, and other electronic devices are dismantled and

separated into casings, anodes, separators, and cathodes. The anode and the cathode are immersed in an *N*-methylpyrrolidone (NMP) solution and treated ultrasonically to peel the cathode material (LFP) and anode material (graphite) from the current collectors (aluminum foil (Al), copper foil (Cu)) based on the "similar miscibility" theory.[35] The resultant cathode material is then recycled using the proposed electrochemical methods by extracting the high-value element lithium, taking advantage of easy controllability and chemical savings of the method, leaving the FP as the precipitate. More importantly, new LFP cathode material is regenerated from the obtained Li and FP. (2) Taking advantage of the wide material selection, the discarded parts from spent LIBs are utilized to fabricate a TENG to fully utilize the spent LIBs. (3) Moreover, the fabricated TENG provides the electricity for the electrochemical reaction, charging of the batteries and sintering of the cathode material to achieve the self-powering ability of the system.

As displayed in Fig. 1b, the electrochemical LFP recycling reactor is mainly composed of anodic oxidation and cathodic reduction (Fig. 1b). In the cathode area, the water of the solution is electrolyzed into hydrogen (H_2) and hydroxyl ions (OH^-) according to reaction (1) on the surface of the platinum foil (Pt) *via* the hydrogen evolution reaction (HER). The OH^- is transported to the anode under the electric field to produce the hypochlorite ion (ClO^-) by reacting with chlorine (Cl_2), which is generated by the oxidation of the chloride ion (Cl^-) on the surface of graphite in the anodic area (reaction (2) and (3)). Taking advantage of the high oxidizability of ClO^-, the lithium ions can be extracted from the spent LFP cathode material, leaving the solid insoluble precipitate FP (reaction (4)), and the ClO^- is reduced back to Cl^-. Meanwhile, the Li^+ ions migrate through the membrane from the anodic to the cathodic compartment to balance the charges. Thus, the spent LFP cathode material is oxidized to $FePO_4$ in the anode and Li^+ ions are enriched in the cathode while obtaining the byproduct hydrogen. The results are supported by the cyclic voltammetry (CV) curve of the LFP cathode material in 0.5 M Li_2SO_4 solution, in which the redox potential of LFP is about 0.52 V (*vs.* standard hydrogen electrode (SHE)) while the oxidation potential of HClO is 1.27 V (*vs.* SHE) (Fig. 1c). It is notable that according to the Pourbaix

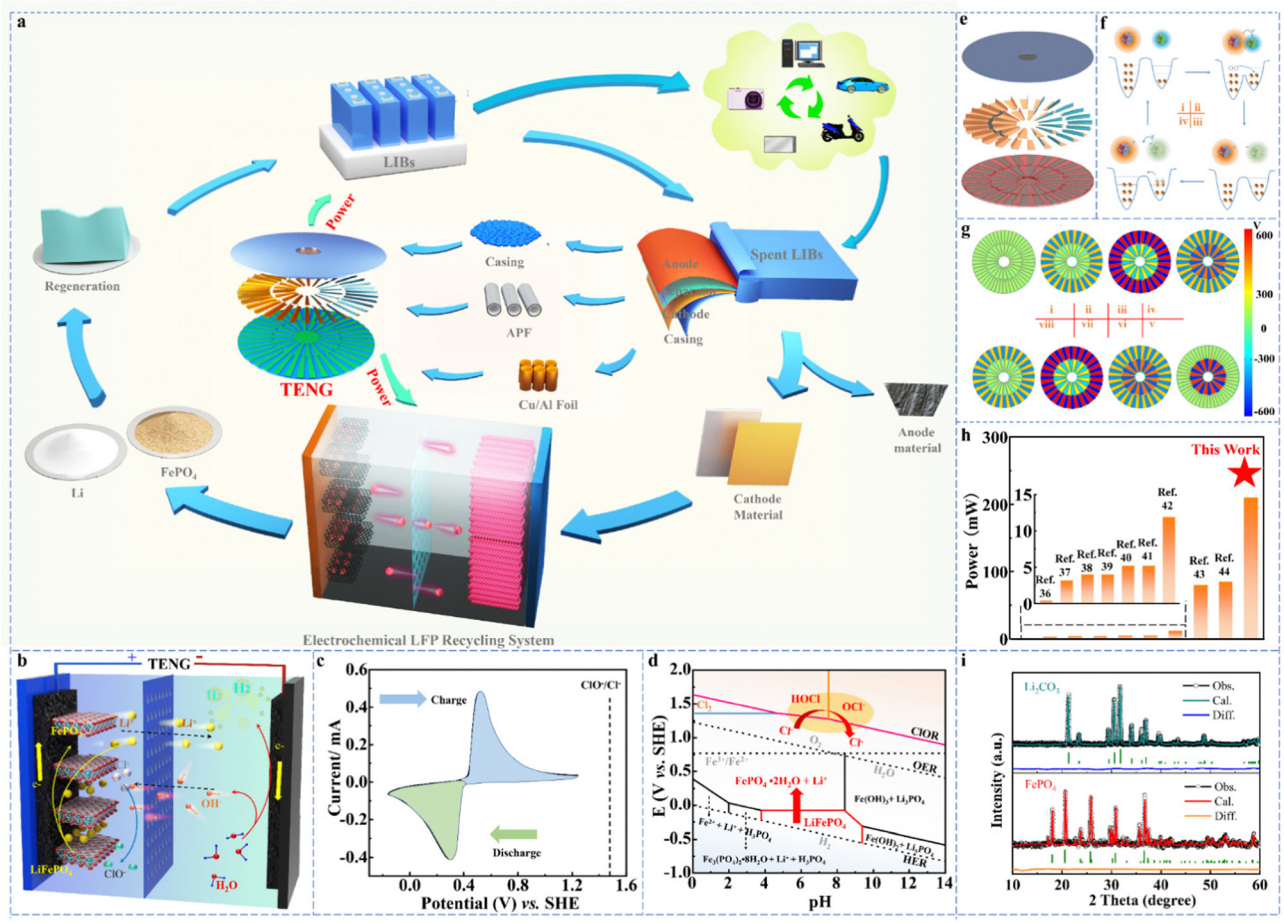

Fig. 1 Design and mechanism of a self-powered system for recycling spent lithium-ion batteries. (a) Schematic illustration of the designed self-powered recycling system for spent LFP batteries. (b) Proposed electrochemical recycling technology of spent LIBs. (c) CV curves of the LFP cathode material in 0.5 M Li_2SO_4 solution. (d) Pourbaix diagram of the LFP–H_2O–Cl system. (e) The fabricated TENG. (f) Electron-cloud-potential-well model of the electron transition process between Cu and PA. (g) Simulation of voltage with COMSOL. (h) Benchmark works for the average power of TENG. (i) Refined XRD results of the recycled Li_2CO_3 and $FePO_4$.

diagram of the LFP–H_2O–Cl system (Fig. 1d), only when the pH of the solution is maintained at around 4–7 can Li be selectively released from the LFP framework and converted to Li^+, maintaining the integrity of the FP framework.[18] Thus, the pH value of the leaching solution was set to 5–6 to avoid acid usage while maintaining high purity.

$$2H_2O + 2e^- \rightarrow 2OH^- + H_2 \quad (1)$$

$$2Cl^- - 2e^- \rightarrow Cl_2 \quad (2)$$

$$Cl_2 + 2OH^- \rightarrow Cl^- + ClO^- + H_2O \quad (3)$$

$$H_2O + ClO^- + 2LiFePO_4 \rightarrow 2Li^+ + Cl^- + 2FePO_4 + 2OH^- \quad (4)$$

The TENG made from discarded components from spent LIBs was rationally designed to harvest wind energy. The rotor is composed of casings and aluminum-plastic film (APF) as a frame and triboelectric layer, respectively, while the stator is made from the recovered printed circuit board (PCB) with recycled Cu deposited on it. Owing to the dual-ring structure of an outer ring (OR-TENG) and inner ring (IR-TENG), the TENG can sufficiently harvest wind energy into electricity (Fig. 1e). The three-layer design (polypropylene (PP)–aluminum (Al)–polyamide (PA)) of the aluminum-plastic film provides two combined friction pairs, Cu/PP and Cu/PA, for optimizing the output of the TENG. The transferred charge (Fig. S1a, ESI†), current (Fig. S1b, ESI†) and voltage (Fig. S1c, ESI†) indicate that the Cu/PA friction pair delivers a higher output, with 70.2 μC m^{-2}, 7.7 μA and 155.8 V, respectively, compared with that of the Cu/PP pair (14.5 μC m^{-2}, 9.76 μA and 94.3 V). The working of the TENG is illustrated by the electron cloud/potential model (Fig. 1f). (i) As the PA and Cu triboelectric layer approach and (ii) come into contact with each other, the electron clouds are overlapped and the energy barriers are lowered. Thus, the electrons transfer from PA to Cu due to the Fermi level differences, and the contact electrification occurs. (iii) After separation, PA is positively charged, and Cu is charged with equal heterogeneous charge. (iv) As the temperature rises, the electrons will either go back to the atoms of the material or be emitted into the air. Therefore, based on the contact electrification and electrostatic induction (Note S1 and Fig. S2, ESI†), an alternative current is generated between the Cu electrodes (Fig. S3, ESI†). The simulation using COMSOL is in good accordance with the voltage results, which indicates that the two rings (OR-TENG and IR-TENG) of the TENG work independently with voltages of 600 V and 400 V, respectively (Fig. 1g). The fabricated TENG with an elastic and self-adaptable structure demonstrates a high average power of 0.21 W compared to many benchmarks in harvesting wind energy (Fig. 1h), including wing-design TENG,[36] transparent and degradable TENG,[37] mail-design TENG,[38] anti-glare panel TENG,[39] dual-rotation shaft TENG,[40] triboelectric-electromagnetic hybridized nanogenerators,[41] rabbit fur-based soft-contact TENG,[42] flower-bud array cotton-based TENG,[43] and elastic rotation TENG.[44] The designed self-powered system based on the TENG can not only achieve energy and chemical savings, but also shows high element selectivities of 99.75% and 99.70% for $FePO_4$ and Li_2CO_3, respectively, based on the refined X-ray diffraction (XRD) patterns (Fig. 1i) and the inductively coupled plasma-atomic emission spectrometer (ICP-AES), demonstrating great social and ecological benefits.

Output performance of the TENG

The transferred charge, current and voltage are vital factors that determine the output performance of a TENG. As shown in Fig. 2a and b, the transferred charge and current of the TENG increase with the rotation speed, with values as high as 1.54 μC and 1.29 mA (1.57 μC and 0.61 μC, and 0.93 mA and 0.36 mA for the OR-TENG and IR-TENG) at a rotary speed of 600 rpm (Fig. S3a–d, ESI†) according to the circuit diagram in Fig. S4a (ESI†). The voltage remains almost stable at about 600 V and 400 V (Fig. S3e–f, ESI†), as also observed in the simulated results using COMSOL (Fig. 1g). The peak power of the TENG exhibits a positive trend with increasing rotary speed (Fig. S3g–h, ESI†), reaching 834.9 mW (544.5 mW and 290.4 mW, respectively, for OR-TENG and IR-TENG) (Fig. 2c) at 600 rpm with an average power of 0.21 W (0.137 W and 0.073 W, respectively, for OR-TENG and IR-TENG) (Fig. 2d). This high output is sufficient to power the electrochemical LIBs recycling system, and is feasible for large-scale application. However, the conversion efficiency of electricity to electrochemical energy is low if the output is used directly for powering the electrochemical reaction. Thus, it is urgent to rectify the high voltage and low current of TENG into a high-current but low-voltage output.

Based on our previous work, transformers (TFs) were considered as a suitable device to rectify the output of the TENG,[25] especially at high frequency. Because the required voltage for the generation of ClO^- is above 1.63 V, rectifying the TENG to the threshold voltage while maintaining large transferred charges and currents is ideal for recycling LIBs. As shown in Fig. 2e and f, the resistances of the TFs increase with increasing frequency and number of TF units. Additionally, owing to the high internal resistance of the TENG, the matched resistance of the TFs should be of the same magnitude of about 5 MΩ to deliver a higher output. Thus, to fully understand the rectification ability of the TFs, the transferred charge, current and voltage after rectification were studied (Fig. S5, ESI†) as per the circuit diagram in Fig. S4b (ESI†), which shows that for the OR-TENG, the transferred charges (Fig. S6, ESI†) and current (Fig. 2g) increase with increasing number of TFs while the voltage declines (Fig. 2h). It is notable that when the number of TF units is 14, the voltage drops to 0.72 V, which makes it hard to generate the ClO^-. Additionally, for the IR-TENG, the transferred charges (Fig. S6, ESI†) and current (Fig. 2g) reach a peak output when 10 TF units are loaded, while the voltage is maintained at 23 V (Fig. 2h). Therefore, for the rectification of the TENG, 12 or 10 of TF units were chosen to deliver the highest output. The peak power of the TENG after rectification is 803 mW (459 mW and 244 mW, respectively, for the OR-TENG and IR-TENG) (Fig. 2i), while an average power of 175.8 mW (114.7 mW and 61.1 mW, respectively, for the OR-TENG and IR-TENG) (Fig. 2j) is maintained, with an efficiency of 83.7% and 83.5%, respectively.

Therefore, the fabricated TENG is capable of powering electrochemical reactions, drive electronics, *etc.* It takes less

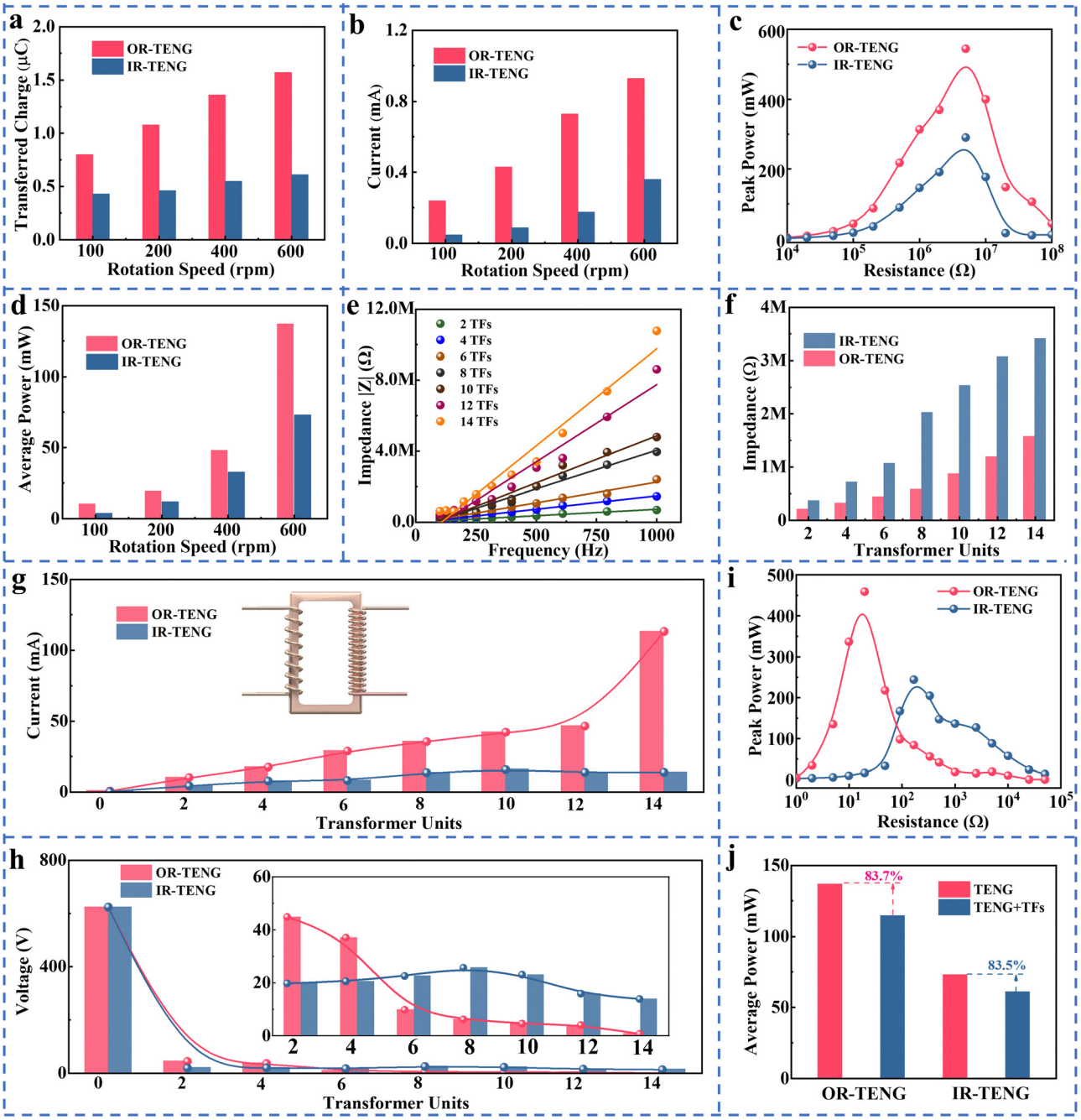

Fig. 2 Output performance of the TENG. (a) Transferred charge, (b) current, (c) peak power and (d) average power of the OR-TENG and IR-TENG at different rotary speeds. (e) Impedance of the transformers at different frequencies and number of units for the OR-TENG and IR-TENG. (f) The impedance of transformers increases with the number of TF units at 600 rpm. (g) The rectified current and (h) voltage at different for different numbers of transformer units. (i) Peak power and (j) average power of the OR-TENG and IR-TENG under the suitable impedance and the conversion efficiency.

than 0.5 s for the OR-TENG and IR-TENG to charge the 2.2 mF capacitors to 2.0 V after rectification, compared with times of 11.3 s and 22.6 s for the OR-TENG and IR-TENG without TFs (Fig. S7a, ESI†). In addition, the TENG was adopted to charge 48 hygrothermograph units for 120 s (Fig. S7b and Video S1, ESI†) according to the circuit diagram in Fig. S7c (ESI†), and a stable working voltage of 1.5 V was maintained (Fig. S7d, ESI†). Furthermore, a wireless temperature and humidity sensor (T & H sensor), a wireless vibration sensor and a wireless light sensor were powered by the TENG (Fig. S8a and b, ESI†) according to the circuit diagram in Fig. S8e (ESI†), and the devices worked steadily (Fig. S8c and Video S1, ESI†). These applications powerfully indicate the high performance of our energy harvesting system.

Working mechanism of electrochemical recycling system

The schematic of the electrochemical LFP recycling system consists of anodic oxidation and cathodic reduction powered by TENG, as

shown in Fig. 3a and Video S2 (ESI†); electrolysis of water to generate H_2 and OH^- occurs in the cathode, while the generation of ClO^- takes place in the anode. Owing to the high oxidizability of ClO^-, the spent LFP is oxidized to Li^+ and FP. As illustrated in Fig. 3b, the cathode electrode is covered with H_2 bubbles with a generation rate of 59 μL min^{-1} (Fig. 3c and Fig. S9, ESI†), which is higher than that in previous works based on TENGs.[45–49]

The recycling performance for LIBs is severely affected by the concentration of ClO^-. In this work, KI was adopted as an indicator to evaluate the reaction progress of ClO^- *via* the yellow color reaction (5) below; the resultant I_2 exhibits a yellow color, and will turn blue when reacted with starch. The voltage of the reaction was around 2.0 V, which is higher than the threshold voltage of 1.63 V for ClOR, indicating the generation

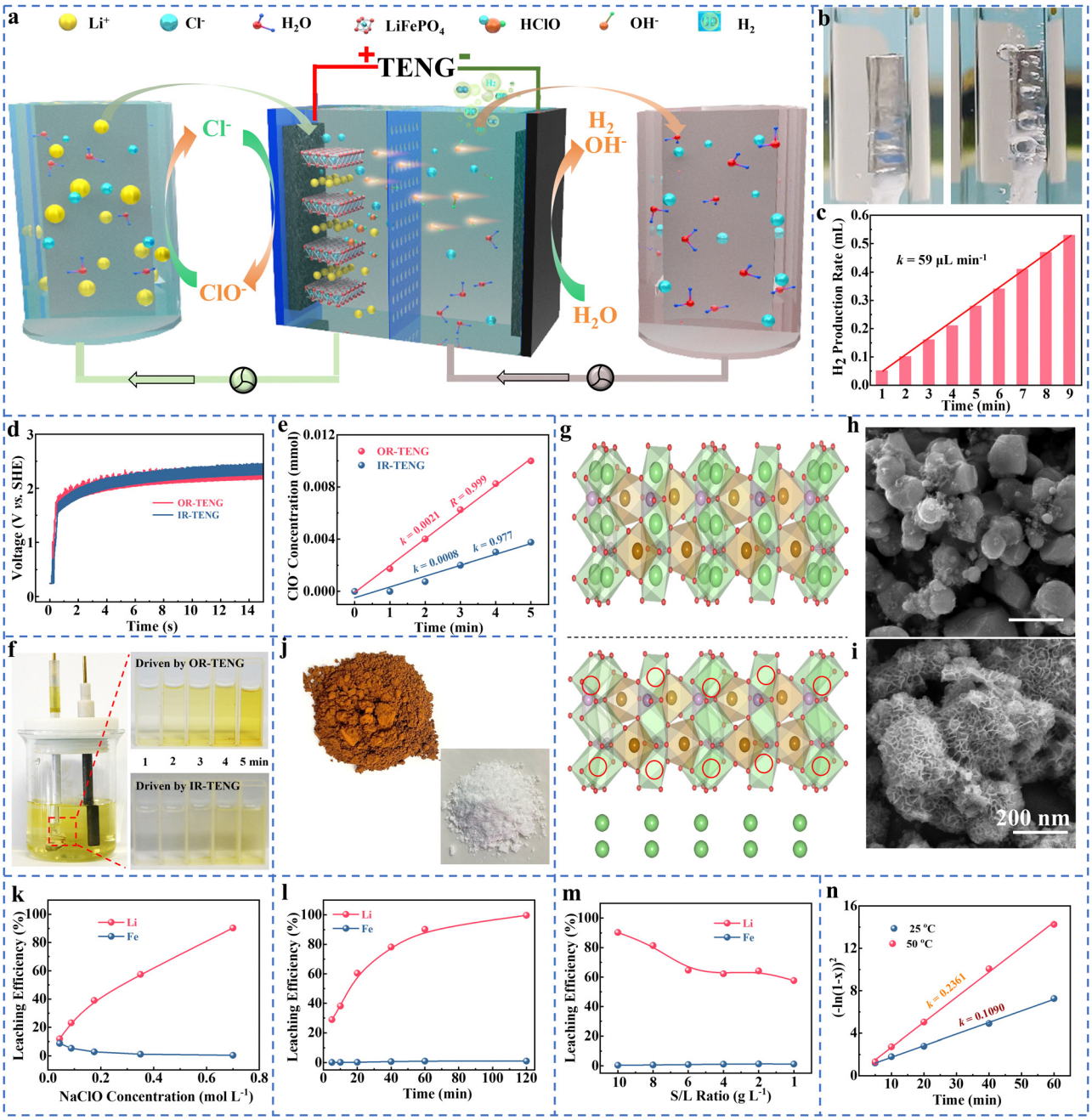

Fig. 3 Working mechanism of the electrochemical recycling system. (a) Schematic illustration of the electrochemical recycling system of spent LFP active materials. (b) Hydrogen being generated in the cathode; (c) the generation rate. (d) Voltage of the electrochemical recycling system, (e) concentration of ClO^- over time, (f) color evolution of the KI-NaCl solution with time as powered using the OR-TENG and IR-TENG. (g) Mechanism of the recycling of the LFP cathode material using ClO^- and SEM images of the LFP material (h) before and (i) after oxidation. (j) Optical image of the obtained FP and Li_2CO_3. Leaching efficiency of Li and Fe as a function of (k) ClO^- concentration, (l) time and (m) *S*/*L* ratio. (n) Leaching kinetics model of the LFP cathode material.

of ClO^- (Fig. 3d). Titration of the reaction solution using sodium thiosulfate suggested that the generation rate of ClO^- is 2.9 μmol min^{-1} (2.1 μmol min^{-1} and 0.8 μmol min^{-1} for the OR-TENG and IR-TENG, respectively) (Fig. 3e), which also has a positive relationship with the charge quantity (Fig. S10a, ESI†). The generation of ClO^- (I_2) was further confirmed from the ultraviolet-visible (UV-Vis) absorption spectrum (Fig. S11a, ESI†), in which a quantitative line between the absorption values and I_2 concentration is obtained according to the Lambert–Beer law (Fig. S11b, ESI†). Because the pH values increase as the reaction occurs (Fig. S10b, ESI†), it is necessary to keep the pH value at 5–6 using hydrochloric acid. The profile of the ClO^- generation is shown by the color change in Fig. 3f. Additionally, the color produced by OR-TENG is darker than that of IR-TENG due to the output difference.

$$2H^+ + ClO^- + 2I^- \rightarrow Cl^- + I_2 + H_2O \quad (5)$$

As displayed in Fig. 3g, Li^+ is extracted from the spent LFP cathode material due to the high oxidation of ClO^-, leaving $FePO_4$ as the

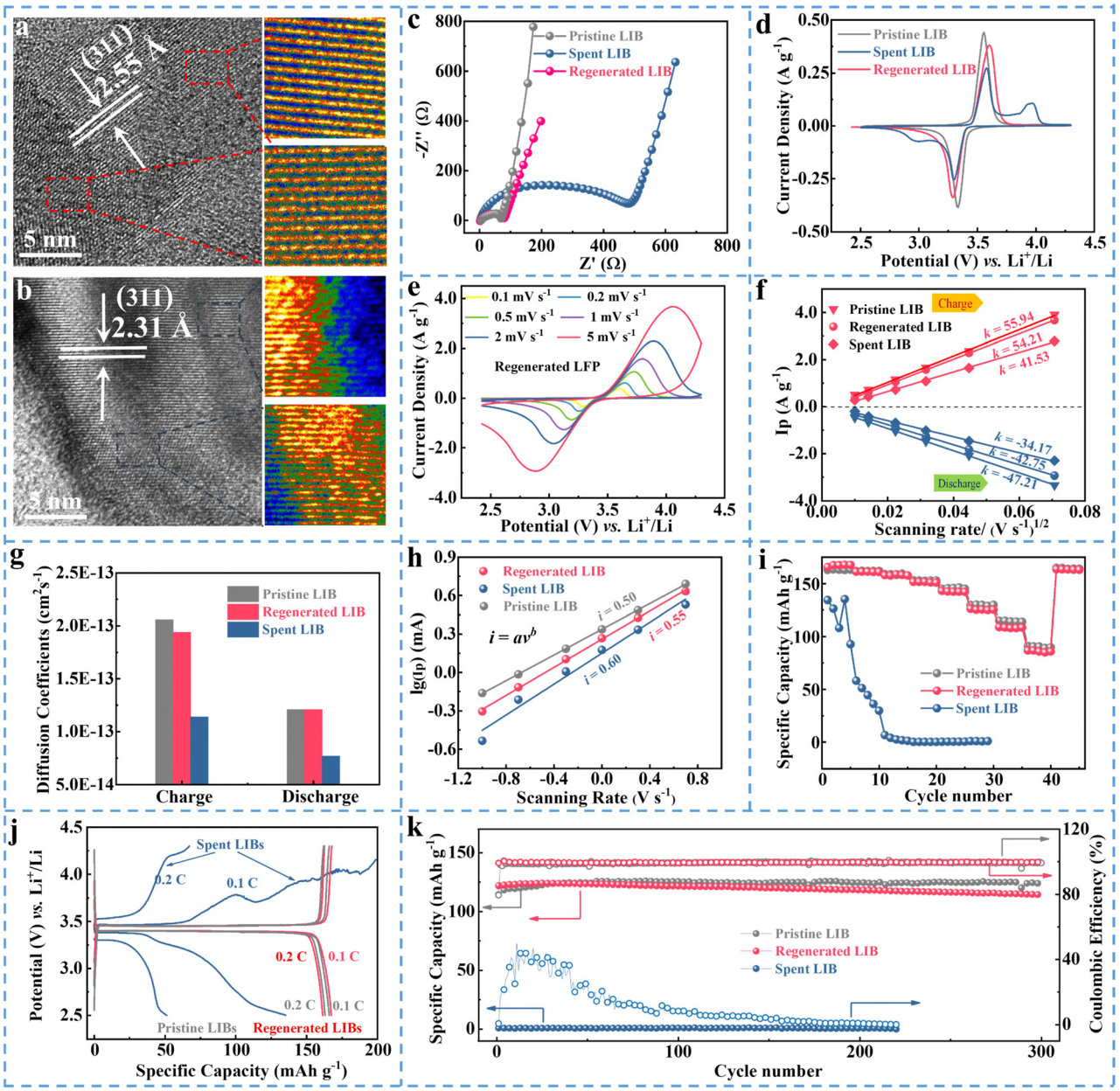

Fig. 4 Regeneration of the LFP cathode material. TEM images of (a) regenerated LFP cathode materials and (b) spent LFP cathode materials. (c) EIS curves and (d) CV curves of the pristine, regenerated and spent LFP cathode materials. (e) CV curves of the regenerated LFP cathode material at different scan rates, (f) the relationship between the peak current and the square root of the scan rate and (g) the calculated Li-ion diffusion coefficients. (h) Electrochemical performance behaviour of the active materials. (i) Rate performance, (j) GCD curves and (k) stability of the pristine, regenerated and spent LFP cathode materials.

deposit. Additionally, the color of the electrochemical leaching reactor containing spent LFP cathode material became brown under 0.7 mol L^{-1} NaClO in 1 hour (Fig. S12, ESI†). Therefore, a flower-like morphology was observed on the surface of $FePO_4$ compared with the spent LFP cathode material (Fig. 3h and i). The $FePO_4$ deposit is obtained, and the Li^+ enriched in the tank (leaching efficiency: 99.82% for 2 hours) is recovered in the form of Li_2CO_3 after centrifugation by adding the saturated Na_2CO_3 solution (Fig. 3j).

The leaching efficiency was further studied, and the results suggest that the leaching efficiency increases with the concentration of ClO^- (Fig. 3k) and reaction time (Fig. 3l), while decreasing with the solid/liquid ratio (Fig. 3m). Moreover, this strategy eliminates the influence of the element iron (Fe), as its concentration is less than 1%. The leaching efficiency was fitted with the leaching time, and the results further suggest that the leaching kinetics of LFP follow a logarithmic rate law model. In addition, according to the reaction rate constants, at leaching temperatures of 25 °C and 50 °C, an activation energy of 24.8 kJ mol^{-1} is obtained using the Arrhenius formula (Note S2 and Fig. 3n, ESI†).[50,51]

Regeneration of LFP LIBs

The regenerated LFP cathode material exhibits a distinct lattice with an interplanar spacing of 2.55 Å assigned to the (311) planes (Fig. 4a), while the spent LFP cathode material acquires a smaller interplanar spacing of 2.31 Å (Fig. 4b). The results are well illustrated by the Fourier transform patterns (IFFT), which indicate that the regenerated LFP cathode material presents a good crystalline structure compared with the seriously disordered lattices in spent LFP. In addition, scanning electron microscopy (SEM) images and energy dispersive X-ray spectroscopy (EDX) also indicate that the elements are well distributed on the regenerated LFP particles (Fig. S13, ESI†). Electrochemical impedance spectroscopy (EIS) indicates that the new generated LFP batteries exhibit a smaller charge-transfer resistance (R_{ct}) of 78 Ω (almost the same as that of the pristine LFP batteries, 69 Ω) compared with a resistance of 500 Ω for the spent LIB (Fig. 4c). Although the overpotential in the cyclic voltammetry (CV) exhibits almost the same trend, the regenerated LFP batteries reduce the side reactions at 4.0 V and 3.0 V during the charge and discharge period that occur on the spent LIB (Fig. 4d). In order to further investigate the Li^+ diffusion coefficient of the LIB and the de-intercalation behavior, CV curves at different charging rates were studied (Fig. 4e and Fig. S14, ESI†). From the fitting line between the peak current and the square root of the scan rate (Fig. 4f), the calculated Li^+ diffusion coefficients (Note S3, ESI†) of the regenerated LIBs are 1.94×10^{-13} cm^2 s^{-1} (charge) and 1.14×10^{-13} cm^2 s^{-1} (discharge), respectively, which are slightly lower than those of the pristine LIBs (2.04×10^{-13} cm^2 s^{-1} for charging and 1.16×10^{-13} cm^2 s^{-1} for discharging) and almost double those of the spent LIB (Fig. 4g). The electrochemical performance behavior of the active materials further indicates that the regenerated LFP cathode material displays a semi-infinite diffusion step (typical battery behavior) rather than surface-controlled energy storage processes (typical capacitor behavior) (Fig. 4h) deriving from the good crystallinity.[52]

The rate performance further suggests that the regenerated LFP cathode material not only exhibits the specific capacity as high as the pristine LFP of 167.8 mA h g^{-1} (0.1C), 161.1 mA h g^{-1} (0.2C), 158.8 mA h g^{-1} (0.5C), 151.7 mA h g^{-1} (1C), 142.4 mA h g^{-1} (2C), 125.5 mA h g^{-1} (5C), 108.6 mA h g^{-1} (10C) and 85.9 mA h g^{-1} (20C), but also presents a good rate ability (Fig. 4i). The results are confirmed by the charge/discharge curves, in which the overpotential of regenerated LIB is much smaller than that of spent LIB (Fig. 4j). Additionally, the stability test proves that the regenerated LIB exhibits a retention of 94.0% with a capacity of 114.6 mA h g^{-1} after 300 cycles at a rate of 5C, which is almost the same as the pristine LIBs (Fig. 4k).

The self-powered system for recycling spent LFP batteries

The TENG fabricated from the accessories of spent LIBs, such as casings, separators, and current collectors, harvests the wind energy in the environment into electricity. By rectifying the high-voltage and low-current output to have high-current and low-voltage characteristics using transformers, a self-powered spent LIB recovery system based on the TENG and electrochemical LIB recycling reactor was assembled (Fig. 5a). Therefore, with the assistance of the windmill, the fabricated self-powered spent LIB recovery system works by harnessing wind energy (Fig. 5b) according to the circuit diagram (Fig. S15a, ESI†). As mentioned above, when the reaction occurs driven by the TENG, the color of the electrochemical reactor will change from colorless (Fig. 5c-i) to brown (Fig. 5c-ii) due to the generation of ClO^- with the assistance of I_2. In order to verify the generation of I_2, starch was added to the solution, which will turn blue when there is iodine. The blue color change verified it (Fig. 5c-iii). The transferred charge (Fig. 5d) and current (Fig. 5e) increased to 41.4 μC (30.4 μC and 11.0 μC for OR-TENG and IR-TENG) and 24.9 mA (21.6 mA and 3.3 mA for OR-TENG and IR-TENG), respectively, and the voltage (Fig. 5f) dropped to several volts (11.5 V and 6.6 V for OR-TENG and IR-TENG) after rectification by the TFs. Additionally, the voltage on the self-powered LIB recycling system is 1.6–1.7 V, which is capable of powering the ClOR reaction (Fig. S15b, ESI†). Fig. 5g further evidences that the output could not only generate ClO^- in the anode electrode as indicated by the yellow color, but also realize its rapid accumulation. As shown in Fig. 5h, the generation rate of ClO^- is as high as 2.4 μmol min^{-1}, while in the cathode electrode, hydrogen is also obtained with a generation rate of 0.047 mL min^{-1} owing to the water electrolysis reaction (Fig. 5i), which realizes the utilization of the dual electrode (Video S2, ESI†).

The latest works in the area of recycling LFP LIBs are summarized in Table S1 (ESI†). The summary suggests that the direct regeneration of spent LFP cathode material is a promising strategy because it avoids the decomposition of LFP. However, a re-lithiation process, including hydrothermal treatment, a sintering process and follow-up sintering at high temperature is required, which leads to high energy consumption.[10,11,53,54] For direct recycling using a molten salt

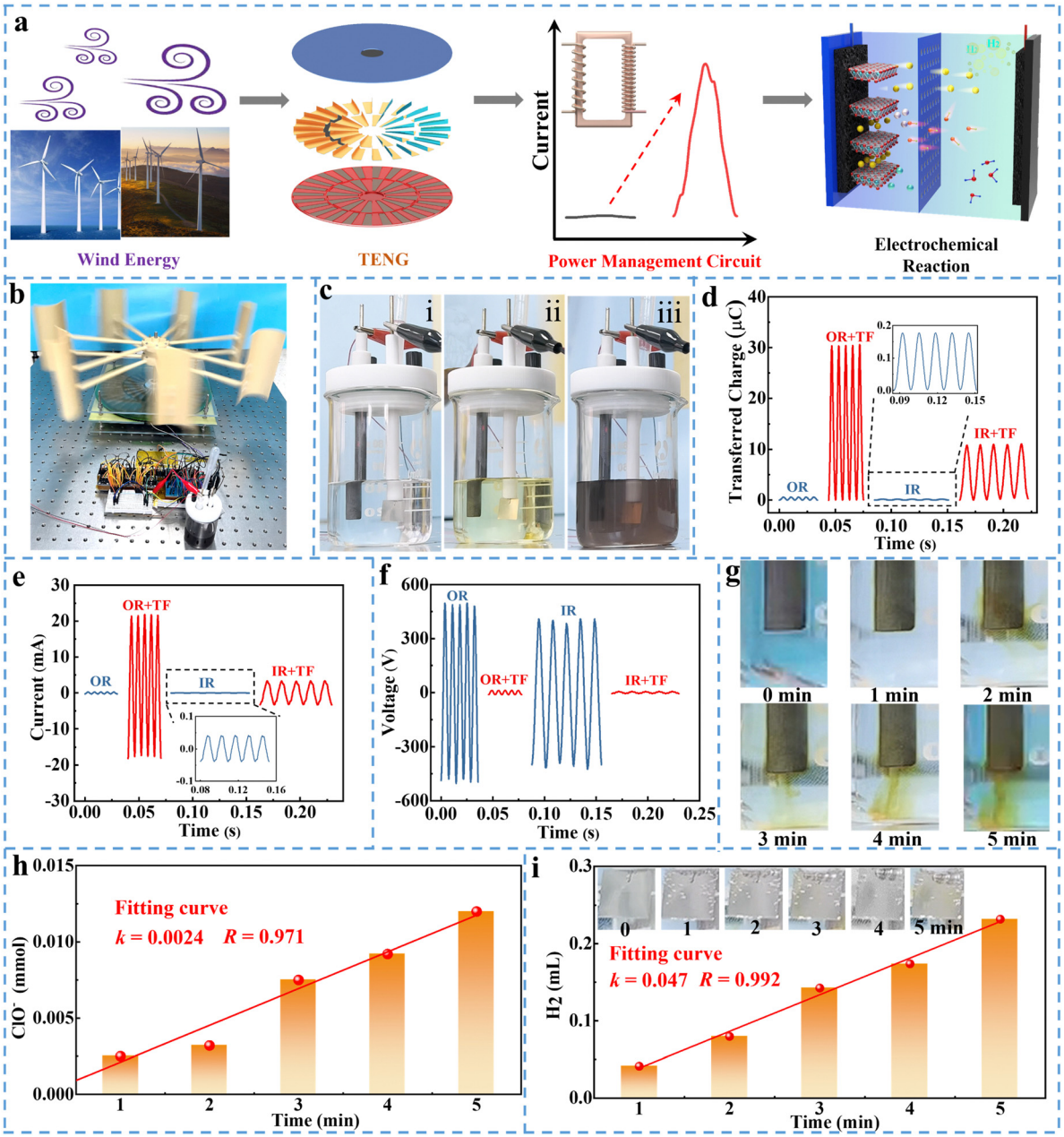

Fig. 5 The self-powered system for recycling spent LFP batteries powered by wind. (a) Schematic illustration and (b) images of the self-powered LFP recovery system. (c) The reaction in the electrochemical reactor: (i) before the reaction, (ii) after the reaction and (iii) verifying the reaction. (d) The transferred charge, (e) current, and (f) voltage before and after rectification by TFs. (g) The generation reaction of ClO^- in the anode and (h) the amount. (i) The amount of generated hydrogen; inset images show the reaction of hydrogen on the cathode electrode.

process, low temperature is favorable for practical use because of the energy savings. However, the additives are pricey and hard to synthesize.[12,55] Electrochemical regeneration by using a prelithiation separator and the oxidation process has been intensively studied. Unfortunately, these processes are limited by their unsustainability in terms of energy and materials.[13,17,56] Additionally, these studies have mainly focused on the cathode material while paying little attention to the anode, casing, separator, and other accessories. Our work reports an electrochemical recycling process for LFP batteries by recycling all the components. Moreover, the fabricated TENG harvests the wind energy to significantly offset the energy input, which is of economic and environmental importance.

Economic evaluation of lithium recycling strategy and prospects

The overall process of the self-powered system for recycling spent LFP batteries is presented in Fig. 6a. Impressively, the common oxidant ClO^- is obtained as a green reagent by electrochemical electrolysis of saline solution without introducing other impurities. The proposed method can significantly simplify the recycling procedure and reduce chemical

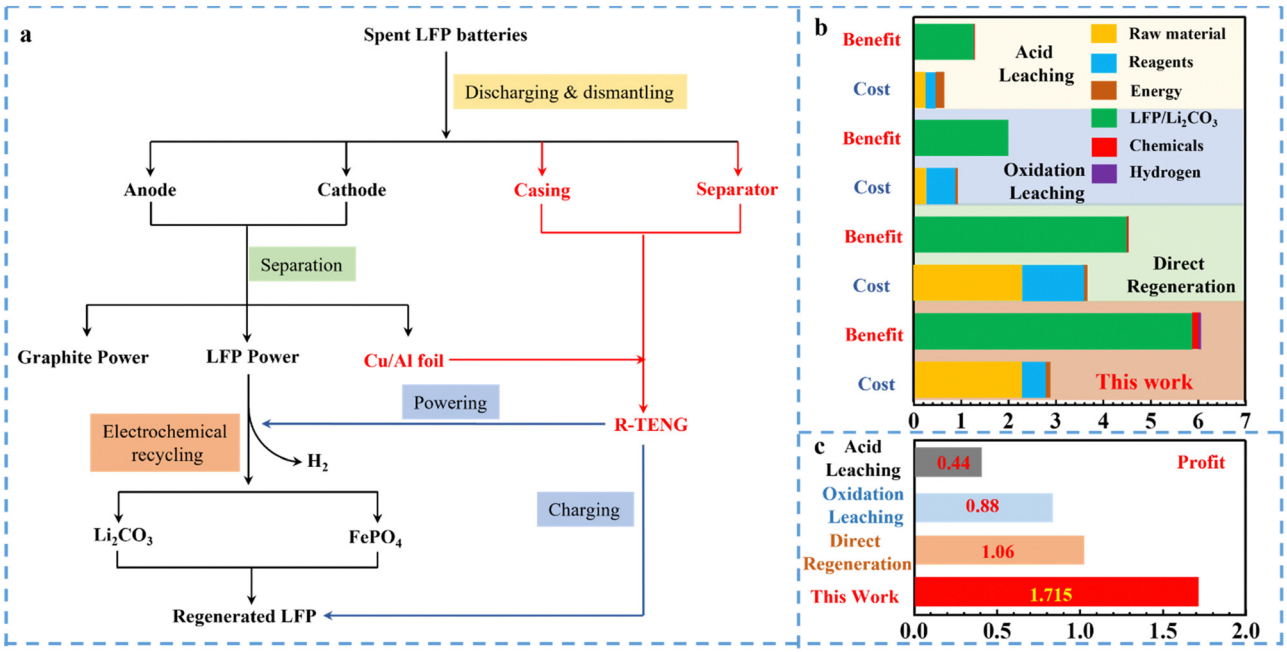

Fig. 6 Process flow diagram and cost assessment. (a) Process flow diagram of the self-powered system for recycling spent LFP batteries. (b) Cost assessment and (c) profit of this work and comparison with conventional methods.

consumption with high selectivity and minimized hazardous waste. Furthermore, by fabricating the TENG, the accessories from spent batteries can be rationally utilized without secondary pollution. More importantly, the fabricated TENG harvests wind energy to generate electricity for powering the electrochemical recycling system and charging the LFP batteries.

A technoeconomic analysis was carried out by considering the market prices of the raw material, reagents, products, and energy consumption that are generated or used in the recovery process of the LFP cathode material. As shown in Fig. 6b and Note S4 (ESI†), taking advantage of the full recovery of the spent LFP, the benefit of this work when recycling 1 kg LFP batteries is \$6.046 due to the pricey spent LFP battery compared with \$4.702, \$1.272 and \$1.959 for the direct regeneration method (Note S5, ESI†),[55] acid leaching method[8] and oxidation leaching method that recycle spent LFP cathode material at low cost.[17] Meanwhile, the cost of this work is \$4.331 compared with \$3.638, \$0.832 and \$1.080 for the direct regeneration, conventional acid leaching method and oxidation leaching method. It is notable that although the reagent NMP is expensive, the cost of this work can be reduced from \$4.331 to \$2.891 due to the reusability of NMP. Additionally, this work results in a higher profit because of the simplified treatment procedure and reduced chemical use. Therefore, the profit of this work is \$1.715 compared with \$1.06, \$0.44 and \$0.88 for the direct regeneration method, acid leaching method and oxidation leaching method, suggesting that the proposed self-powered system is of economic importance (Fig. 6c).

Conclusions

Aiming to address the environmental crisis resulting from spent batteries, this work proposes an innovative self-powered system for recycling spent LFP based on a triboelectric nanogenerator (TENG) with high selectivity, self-powering, a simplified procedure, and a high profit. With the electrochemically generated Cl^-/ClO^- pair as the redox mediator, LFP is readily broken down into $FePO_4$ and Li^+ *via* the redox targeting reaction without extra chemicals. The recycled Li_2CO_3 and $FePO_4$ exhibit purities of 99.70% and 99.75%, respectively. Furthermore, the new LFP cathode material is regenerated from the recycled Li_2CO_3 and $FePO_4$ exhibits enhanced electrochemical performance, a doubled lithium-ion coefficient and superior cyclic stability. Benefiting from the wide material selection, a TENG made from discarded components including casings, aluminum-plastic films and current collectors from LIBs was designed, which harvests wind energy into electricity, delivering an output of 0.21 W for powering the electrochemical recycling system. Combining the self-powered features, simplified treatment procedure and high profit, the proposed self-powered system for recycling spent LFP exhibits feasibility in commercial applications.

Experimental section

LFP battery dismantling

The spent LFP batteries are manually dismantled into casings, cathodes, anodes, and separators after being immersed in NaCl solution for 24 h. Then, NMP is added into the cathode and anode to separate the active materials (LFP cathode material and graphite anode material) from the current collectors (Al foil for the cathode and Cu foil for anode) by dissolving the PVDF binder. The graphite, LFP cathode material, Al foil, Cu foil, casing, and separators are recovered after cleaning and drying.

Electrochemical recycling of LFP cathode material

The LFP cathode material is mixed in 0.6 mol L^{-1} NaCl solution and hydrochloric acid is used to maintain the pH at 6. In the cathode, platinum (Pt) is used for water electrolysis to obtain the hydrogen and hydroxyl. In the anode with graphite as the electrode, Cl^- is oxidized into ClO^- and then oxidizes the LFP cathode material. KI is added to observe the reaction phenomenon when needed. As the reactions proceed, Li^+ is enriched in the solutions and FP is obtained using filtering. Afterwards, Li_2CO_3 is obtained by adding saturated Na_2CO_3 by filtering the solvent after concentration.

Regeneration of the LFP cathode material

The recycled FP and Li_2CO_3 are mixed with a molar ratio of 1 : 0.505. The mixtures are first calcined at 350 °C for 2 h. The obtained precursor is sintered again at 650 °C for 6 h after grinding under a nitrogen atmosphere. The resultant LFP cathode material is cooled naturally, ground and stored in a vacuum package.

Fabrication of the TENG

The TENG with a radius of 15 cm is composed of a rotor and a stator. In the stator part, a dual-ring design is used to harvest sufficient wind energy, in which 24 pairs and 48 pairs of copper grids are designed in the inner ring and outer ring, respectively, on the PCB. It is notable that the frame is fabricated with recycled PVC casings and the copper grids are chemically deposited on the PCB board using the recycled Cu foils. The corresponding stator part is composed of 24 pieces and 48 pieces of aluminum-plastic films in the inner ring and outer ring, respectively.

Output measurement of the TENG

The transferred charge, short-circuit current and power are tested using a programmable electrometer (Keithley model 6514); the voltage is measured by a domain oscilloscope (MDO3024). The rotation speeds are controlled using a rotation motor (86HSE8.5 H-B32).

Characterization of the electrochemical recycling system

The electrochemical performance of the LFP cathode material is tested in a three-electrode system using a Versatile Multichannel Potentiostat 2/Z (VMP2, BioLogic) with 0.5 M Li_2SO_4/NaCl solution, a platinum foil and a saturated calomel electrode (SCE) as the electrolyte, counter electrode, and reference electrode, respectively. The potential of the reaction *vs.* SHE (V_{SHE}) is calculated using the formula $V_{SHE} = V_{SCE} + 0.2415$. The UV-Vis spectra in the range of 500–180 nm are used to verify the ClO^- by adding KI using an ultraviolet-visible spectrophotometer (UV-2600, Shimadzu). The volume of the hydrogen obtained is tested using a displacement method. The amount of ClO^- generated is calculated using an oxidation–reduction titration method with sodium thiosulfate as the titrating solution and starch as the indicator under the assistance of KI. The Li and Fe contents in the solutions are determined using an inductively coupled plasma-atomic emission spectrometer (ICP-AES, Optima 3000DV, PerkinElmer Instrument). The leaching efficiency of Li is calculated as follows:

$$\frac{\text{Content of Li in the leachate}}{\text{Total content of Li in the cathode}} \times 100\%$$

Characterization of regenerated LFP cathode material

A powder X-ray diffractometer (RIGAKU Ultima IV), a high-resolution field emission scanning electron microscope (RESEM, JEOL, JSM-7610FPlus, Japan) and a transmission electron microscope (TEM, JEOL, JEM-2100F, Japan) are used to characterize the crystal phases, particle morphology, and crystal lattice of the regenerated LFP, respectively. The electrochemical performance of the regenerated LFP is tested using a Versatile Multichannel Potentiostat 2/Z (VMP2, BioLogic) by assembling CR2016 half-cells (80 wt% regenerated LFP811 cathode material, 10 wt% super P and 10 wt% PVDF binder).

Author contributions

B. Z. conceived the idea, designed the experiments, and performed data measurements. L. H., R. Z., Y. L., X. X., and S. H. analyzed the data. C. Z. and Z. Z. helped with the experiments. B. Z., L. Z., and J. W. drafted the manuscript. B. Z., J. W., and Z. L. W. supervised this work. All the authors discussed the results and commented on the manuscript.

Conflicts of interest

There are no conflicts to declare.

Acknowledgements

The research is supported by the financial support of the National Key R & D Project from Minister of Science and Technology (2021YFA1201602), the Innovation Project of Ocean Science and Technology (22-3-3-hygg-18-hy), the National Nature Science Foundation of China (No. 61774016, 21773009, U21A20147, and 22109013), the China Postdoctoral Science Foundation (2022M713110), the Fundamental Research Funds for the Central Universities (E1E46802), and the Bei-jing Municipal Science & Technology Commission (Z171100000317001, Z171100002017017, and Y3993113DF).

References

1 M. Ryu, Y. K. Hong, S. Y. Lee and J. H. Park, *Nat. Commun.*, 2023, **14**, 1316.
2 W. Deng, X. Yin, W. Bao, X. F. Zhou, Z. Y. Hu, B. Y. He, B. Qiu, Y. S. Meng and Z. P. Liu, *Nat. Energy*, 2022, **7**, 1031–1041.
3 D. Hou, Z. R. Xu, Z. J. Yang, C. G. Kuai, Z. J. Du, C. J. Sun, Y. Ren, J. Liu, X. H. Xiao and F. Lin, *Nat. Commun.*, 2022, **13**, 3437.
4 L. Xu and C. V. Thompson, *J. Mater. Chem. A*, 2020, **8**, 21872–21881.
5 G. Harper, R. Sommerville, E. Kendrick, L. Driscoll, P. Slater, R. Stolkin, A. Walton, P. Christensen, O. Heidrich, S. Lambert,

A. Abbott, K. Ryder, L. Gaines and P. Anderson, *Nature*, 2019, **575**, 75–86.
6 P. Meshram, B. D. Pandey and T. R. Mankhand, *Hydrometallurgy*, 2014, **150**, 192–208.
7 P. P. Xu, D. H. S. Tan, B. L. Jiao, H. P. Gao, X. L. Yu and Z. Chen, *Adv. Funct. Mater.*, 2023, **33**, 2213168.
8 J. L. Zhang, J. T. Hu, Y. B. Liu, Q. K. Jing, C. Yang, Y. Q. Chen and C. Y. Wang, *ACS Sustainable Chem. Eng.*, 2019, **7**, 5626–5631.
9 Y. Lu, K. Peng and L. Zhang, *ACS EST. Eng.*, 2022, **2**, 586–605.
10 P. Xu, Q. Dai, H. Gao, H. Liu, M. Zhang, M. Li, Y. Chen, K. An, Y. S. Meng, P. Liu, Y. Li, J. S. Spangenberger, L. Gaines, J. Lu and Z. Chen, *Joule*, 2020, **4**, 2609–2626.
11 X. Liu, M. Wang, L. Deng, Y.-J. Cheng, J. Gao and Y. Xia, *Ind. Eng. Chem. Res.*, 2022, **61**, 3831–3839.
12 G. Ji, J. Wang, Z. Liang, K. Jia, J. Ma, Z. Zhuang, G. Zhou and H.-M. Cheng, *Nat. Commun.*, 2023, **14**, 584.
13 M. Fan, Q. H. Meng, X. Chang, C. F. Gu, X. H. Meng, Y. X. Yin, H. L. Li, L. J. Wan and Y. G. Guo, *Adv. Energy Mater.*, 2022, **12**, 2103630.
14 Q. Jing, J. Zhang, Y. Liu, W. Zhang, Y. Chen and C. Wang, *ACS Sustainable Chem. Eng.*, 2020, **8**, 17622–17628.
15 Z. Liu, C. Zhang, M. Ye, H. Li, Z. Fu, H. Zhang, G. Wang and Y. Zhang, *ACS Appl. Energy Mater.*, 2022, **5**, 14323–14334.
16 J. Yu, X. Wang, M. Zhou and Q. Wang, *Energy Environ. Sci.*, 2019, **12**, 2672–2677.
17 X. Qiu, B. Zhang, Y. Xu, J. Hu, W. Deng, G. Zou, H. Hou, Y. Yang, W. Sun, Y. Hu, X. Cao and X. Ji, *Green Chem.*, 2022, **24**, 2506–2515.
18 K. Liu, M. M. Wang, Q. Z. Zhang, Z. B. Xu, C. Labianca, M. Komarek, B. Gao and D. C. W. Tsang, *J. Hazard. Mater.*, 2023, **445**, 130502.
19 Z. Xiao, L. Gao, S. Su, D. Li, L. Cao, L. Ye, B. Zhang, L. Ming and X. Ou, *Mater. Today Energy*, 2021, **21**, 100821.
20 B. Zhang, L. He, R. Zhang, W. Yuan, J. Wang, Y. Hu, Z. Zhao, L. Zhou, J. Wang and Z. L. Wang, *Adv. Energy Mater.*, 2023, **13**, 2301353.
21 Y. Liu, D. Liu, C. Gao, X. Zhang, R. Yu, X. Wang, E. Li, Y. Hu, T. Guo and H. Chen, *Nat. Commun.*, 2022, **13**, 7917.
22 Y. Feng, X. Liang, J. Han, K. Han, T. Jiang, H. Li and Z. L. Wang, *Nano Lett.*, 2021, **21**, 5633–5640.
23 M. Z. Wu, W. X. Guo, S. G. Dong, A. D. Liu, Y. H. Cao, Z. J. Xu, C. J. Lin and J. Zhang, *npj Mater. Degrad.*, 2022, **6**, 73.
24 C. Zhang, B. Zhang, W. Yuan, O. Yang, Y. Liu, L. He, Z. Zhao, L. Zhou, J. Wang and Z. L. Wang, *ACS Appl. Mater. Interfaces*, 2022, **14**, 8605–8612.
25 B. Zhang, C. Zhang, O. Yang, W. Yuan, Y. Liu, L. He, Y. Hu, Z. Zhao, L. Zhou, J. Wang and Z. L. Wang, *ACS Nano*, 2022, **16**, 15286–15296.
26 S. Li, J. Jiang, N. Zhai, J. Liu, K. Feng, Y. Chen, Z. Wen, X. Sun and J. Zhong, *Nano Energy*, 2022, **93**, 106870.
27 S. Liu, Y. Liu, Y. Chen, S. Wang, C. Men and S. Gao, *ACS Appl. Mater. Interfaces*, 2022, **14**, 17426–17433.
28 S. Gao, Y. Chen, J. Su, M. Wang, X. Wei, T. Jiang and Z. L. Wang, *ACS Nano*, 2017, **11**, 3965–3972.
29 G. Khandelwal, N. Raj and S. J. Kim, *Nano Today*, 2020, **33**, 100882.
30 Y. Li, Z. Zhao, Y. Gao, S. Li, L. Zhou, J. Wang and Z. L. Wang, *ACS Appl. Mater. Interfaces*, 2021, **13**, 30776–30784.
31 G. M. Rani, C. M. Wu, K. G. Motora and R. Umapathi, *J. Cleaner Prod.*, 2022, **363**, 132532.
32 M. A. Jalili, Z. Khosroshahi, N. R. Kheirabadi, F. Karimzadeh and M. H. Enayati, *Nano Energy*, 2021, **90**, 106581.
33 M. Li, W. Y. Cheng, Y. C. Li, H. M. Wu, Y. C. Wu, H. W. Lu, S. L. Cheng, L. Li, K. C. Chang, H. J. Liu, Y. F. Lin, L. Y. Lin and Y. C. Lai, *Nano Energy*, 2021, **79**, 105405.
34 K. Q. Xia, Z. Y. Zhu, J. M. Fu, Y. M. Li, Y. Chi, H. Z. Zhang, C. L. Du and Z. W. Xu, *Nano Energy*, 2019, **60**, 61–71.
35 K. Du, E. H. Ang, X. Wu and Y. Liu, *Energy Environ. Mater.*, 2022, **5**, 1012–1036.
36 H. Zheng, L. Li, M. H. Haider, D.-L. Wen, P. Zhi, C. Tu, X. Ma, J. Xu, Z. Wang and X. Zhang, *Nano Energy*, 2022, **101**, 107627.
37 S. Dai, X. Li, C. Jiang, Q. Zhang, B. Peng, J. Ping and Y. Ying, *Nano Energy*, 2022, **91**, 106686.
38 D. Liu, C. Y. Li, P. F. Chen, X. Zhao, W. Tang and Z. L. Wang, *Adv. Energy Mater.*, 2023, **13**, 2202691.
39 E. Su, H. Li, J. Zhang, Z. Xu, B. Chen, L. N. Y. Cao and Z. L. Wang, *Adv. Funct. Mater.*, 2023, 2214934.
40 S. Yong, J. Y. Wang, L. J. Yang, H. Q. Wang, H. Luo, R. J. Liao and Z. L. Wang, *Adv. Energy Mater.*, 2021, **11**, 2101194.
41 S. Yong, H. Q. Wang, Z. N. Lin, X. S. Li, B. Y. Zhu, L. J. Yang, W. B. Ding, R. J. Liao, J. Y. Wang and Z. L. Wang, *Adv. Energy Mater.*, 2022, **12**, 2202469.
42 J. Han, Y. Feng, P. Chen, X. Liang, H. Pang, T. Jiang and Z. L. Wang, *Adv. Funct. Mater.*, 2021, **32**, 2108580.
43 C. Men, X. Liu, Y. Chen, S. Liu, S. Wang and S. Gao, *Nano Energy*, 2022, **101**, 107578.
44 C. G. Zhang, Y. B. Liu, B. F. Zhang, O. Yang, W. Yuan, L. X. He, X. L. Wei, J. Wang and Z. L. Wang, *ACS Energy Lett.*, 2021, **6**, 1490–1499.
45 Q. Jiang, Y. Han, W. Tang, H. Zhu, C. Gao, S. Chen, M. Willander, X. Cao and Z. L. Wang, *Nano Energy*, 2015, **15**, 266–274.
46 W. Tang, Y. Han, C. B. Han, C. Z. Gao, X. Cao and Z. L. Wang, *Adv. Mater.*, 2015, **27**, 272–276.
47 A. Wei, X. Xie, Z. Wen, H. Zheng, H. Lan, H. Shao, X. Sun, J. Zhong and S. T. Lee, *ACS Nano*, 2018, **12**, 8625–8632.
48 X. Wei, Z. Wen, Y. Liu, N. Zhai, A. Wei, K. Feng, G. Yuan, J. Zhong, Y. Qiang and X. Sun, *Nanomicro Lett.*, 2020, **12**, 88.
49 Y. Yang, H. Zhang, Z.-H. Lin, Y. Liu, J. Chen, Z. Lin, Y. S. Zhou, C. P. Wong and Z. L. Wang, *Energy Environ. Sci.*, 2013, **6**, 2429–2434.
50 B. Zhu, Y. Zhang, Y. Zou, Z. Yang, B. Zhang, Y. Zhao, M. Zhang, Q. Meng and P. Dong, *J. Environ. Manage.*, 2021, **300**, 113710.
51 X. Zhang, H. Cao, Y. Xie, P. Ning, H. An, H. You and F. Nawaz, *Sep. Purif. Technol.*, 2015, **150**, 186–195.
52 L. Xu, M. J. Chon, B. Mills and C. V. Thompson, *J. Power Sources*, 2022, **552**, 232260.
53 K. Jia, J. Ma, J. Wang, Z. Liang, G. Ji, Z. Piao, R. Gao, Y. Zhu, Z. Zhuang, G. Zhou and H. M. Cheng, *Adv. Mater.*, 2023, **35**, 2208034.
54 B. Chen, M. Liu, S. Cao, H. Hu, G. Chen, X. Guo and X. Wang, *J. Alloys Compd.*, 2022, **924**, 166487.
55 Z. Wang, H. Xu, Z. Liu, M. Jin, L. Deng, S. Li and Y. Huang, *J. Mater. Chem. A*, 2023, **11**, 9057–9065.
56 D. Peng, X. Wang, S. Wang, B. Zhang, X. Lu, W. Hu, J. Zou, P. Li, Y. Wen and J. Zhang, *Green Chem.*, 2022, **24**, 4544–4556.

